








## PAPER

View Article Online  
View Journal | View Issue

# Diffractive mirrors for neutral-atom matter-wave optics†

Lee Yeong Kim, <sup>‡a</sup> Do Won Kang, <sup>‡b</sup> Sanghwan Park, <sup>c</sup>  
Seongyeop Lim, <sup>c</sup> Jangwoo Kim, <sup>d</sup> Wieland Schöllkopf <sup>e</sup>  
and Bum Suk Zhao <sup>\*ab</sup>

Received 23rd November 2023, Accepted 29th January 2024

DOI: 10.1039/d3fd00155e

Mirrors for atoms and molecules are essential tools for matter-wave optics with neutral particles. Their realization has required either a clean and atomically smooth crystal surface, sophisticated tailored electromagnetic fields, nanofabrication, or particle cooling because of the inherently short de Broglie wavelengths and strong interactions of atoms with surfaces. Here, we demonstrate reflection of He atoms from inexpensive, readily available, and robust gratings designed for light waves. Using different types of blazed gratings with different periods, we study how microscopic and macroscopic grating properties affect the mirror performance. A holographic grating with 417 nm period shows reflectivity up to 47% for He atoms, demonstrating that commercial gratings can serve as mirrors for thermal energy atoms and molecules. We also observe reflection of He<sub>2</sub> and He<sub>3</sub> which implies that the grating might also function as a mirror for other breakable particles that, under typical conditions, do not scatter nondestructively from a solid surface such as, e.g., metastable atoms or antihydrogen atoms.

## 1 Introduction

In 1923, Louis de Broglie postulated the wave nature of particles in his thesis, introducing the concept of matter-wave wavelength, which is inversely proportional to the product of the particle's mass and velocity. In the same decade, his idea was experimentally confirmed for electrons (1927)<sup>1</sup> and atoms of thermal

<sup>a</sup>Department of Physics, Ulsan National Institute of Science and Technology (UNIST), Ulsan 44919, Korea. E-mail: zhao@unist.ac.kr

<sup>b</sup>Department of Chemistry, Ulsan National Institute of Science and Technology (UNIST), Ulsan 44919, Korea

<sup>c</sup>School of Energy and Chemical Engineering, Ulsan National Institute of Science and Technology (UNIST), Ulsan 44919, Korea

<sup>d</sup>Pohang Accelerator Laboratory, POSTECH, Pohang, Gyeongbuk 37673, Korea

<sup>e</sup>Fritz-Haber-Institut der Max-Planck-Gesellschaft, Faradayweg 4-6, 14195 Berlin, Germany. E-mail: wschoell@fhi-berlin.mpg.de

† Electronic supplementary information (ESI) available. See DOI: <https://doi.org/10.1039/d3fd00155e>

‡ L. Y. K. and D. W. K. contributed equally to this work.



energy (1930)<sup>2</sup> sequentially. Shortly after that, the short wavelength due to the small mass of the electron and the expected analogy of matter-wave optics to photon optics led to the development of the electron-optical imaging system, the first electron microscope (1932).<sup>3</sup> This rapid development was possible because the strong interaction of electrons with static electromagnetic fields allows easy focusing of electrons. Since then, the electron microscope has become an indispensable tool in various fields of modern science and engineering, including physics, material science, chemistry, life sciences, and chemical engineering.

As for neutral atoms, however, their interaction with fields is not strong enough to manipulate them easily. This difficulty has delayed the establishment of the atom microscope. Only in the twenty-first century were two types of scanning helium microscopes (SHeM) in operation. In these apparatuses, probe atoms, typically thermal energy (5–100 meV) neutral helium atoms, are either collimated by a pinhole<sup>4–9</sup> or focused by a Fresnel zone plate.<sup>10–13</sup> Spatial resolutions of 0.35  $\mu\text{m}$  (ref. 5) and 1  $\mu\text{m}$  (ref. 13) have been reported, respectively. The new scanning microscopes can image delicate surfaces such as biological samples, nonconducting material, and organic films, even under the influence of electric or magnetic fields.<sup>7</sup> Such surfaces are challenging to image with the electron microscope. On the other hand, the weak interaction, which was a hurdle for controlling atoms, is beneficial for interferometry applications. Therefore, atom interferometry has found numerous applications in modern sciences, of which examples are inertial sensors, the detection of the  $\text{He}_2$  molecule, and polarizability measurements.<sup>14</sup> These microscopes and interferometers employing atoms and molecules are based mostly on their transmission through nanostructures such as Fresnel zone plates and transmission gratings, pinholes, or non-material diffraction gratings formed by a laser field. However, these instruments surprisingly rarely use mirrors, which are ubiquitous components in traditional optical instruments.

On the other hand, various mirrors for atoms and molecules have been suggested, which can be categorized into three types according to the underlying reflection mechanisms: classical-reflection mirrors, quantum-reflection mirrors, and mirrors based on multiple edge-diffraction reflection. In the classical description of scattering from a solid surface, the particle is reflected when it reaches the classical turning point of the particle–surface interaction potential. That is the well-defined point along the particle trajectory where the particle's kinetic energy has been fully converted into potential energy. In the quantum mechanical picture, on the other hand, partial reflection of the particle's wave can occur at both positive and negative potential slopes without reaching a classical turning point. A familiar example of this counterintuitive quantum phenomenon is the partial reflection of a wave from a downward potential step, an illustrative problem found in most quantum mechanics textbooks. This effect can occur at the attractive long-range branch of the particle–surface potential and is referred to as quantum reflection (or quantum threshold reflection). The probability of quantum reflection depends strongly on the incident particle's kinetic energy. It approaches unity in the limit of vanishing incident energy. Another intriguing non-classical reflection mechanism is multiple edge-diffraction reflection. This occurs when particles scatter from a periodic array of half planes, as shown schematically in the lower part of Fig. 2(a). Here reflection is mediated solely by diffraction of the matter waves at the half plane edges. The edges of a blazed



optical diffraction grating can effectively serve as an array of half planes, as indicated in the upper part of Fig. 2(a). The three reflection mechanisms can be differentiated experimentally through different dependencies of their reflectivity on parameters such as incidence angle, initial kinetic energy of the particle, type of particle, surface structure, and surface temperature.

Atomically smooth solid surfaces, namely crystal surfaces, were the first atomic/molecular mirrors dating back to the earliest atom optics experiments. Using a LiF crystal surface, Estermann and Stern proved the wave-type properties of atoms and molecules.<sup>2</sup> Since then, atom scattering *via classical reflection* from a crystal surface has flourished as a tool for studying surface physics and chemistry.<sup>15,16</sup> In these experiments, an atomically smooth surface is generally necessary to reflect thermal energy atoms and molecules with a speed of hundreds of  $\text{m s}^{-1}$  since their de Broglie wavelengths are on the order of 100 pm. Alternatively, magnetic fields,<sup>17–19</sup> electrostatic fields,<sup>20</sup> and electromagnetic waves<sup>21</sup> have been used as mirrors for slow atoms and molecules of relatively long wavelengths. The underlying physics of these mirrors is also classical reflection of atoms and molecules slower than  $30 \text{ m s}^{-1}$  from the interaction potential between the particle and field.

Liquid helium films coated on a solid surface<sup>22–24</sup> and, subsequently, flat<sup>25–29</sup> and structured solid surfaces<sup>30,31</sup> have served as *quantum-reflection* mirrors. Since quantum reflection allows an atom or molecule to be reflected from a surface before reaching the classical turning point,<sup>32,33</sup> the quantum-reflection mirror does not need to be as atomically smooth as the crystal-surface mirror. However, its reflectivity is negligible for typical conditions of thermal kinetic energies and near-normal incidence. Observable quantum-reflection probabilities can only be expected if the incident velocity component normal to the surface is exceedingly small. Accordingly, the first quantum-reflection mirrors were demonstrated for slow atoms incident at grazing incidence angles of 1–10 mrad.<sup>22,25</sup> Under normal incidence these mirrors only work for ultracold atoms of minimal velocities, such as a Bose–Einstein condensate.<sup>27,31</sup> Grazing incidence, on the contrary, allows thermal atoms to be quantum reflected from various surfaces.<sup>26,29</sup> Furthermore, a curved quantum-reflection mirror made a thermal-energy beam of  $^4\text{He}$  atoms one-dimensionally focused to a spot width below  $2 \mu\text{m}$ ,<sup>28</sup> which could become a focusing element of a scanning He microscope.

Multiple edge-diffraction reflection (MEDR), which is a coherent reflection process of the particle's wave,<sup>34</sup> was first demonstrated with nanoscale ridged structures for ultra-cold atoms under grazing incidence conditions.<sup>35,36</sup> An experimental analysis of the diffraction efficiencies for He and  $\text{D}_2$  beams reflected from a square-wave grating composed of  $10 \mu\text{m}$  wide strips separated by  $400 \mu\text{m}$  confirmed the MEDR model description.<sup>37</sup> Yet, in order to achieve high reflection efficiency, as needed for a useful mirror, finer ridged surfaces prepared by nanofabrication techniques will be needed.

Each type of mirror comes with specific challenges. For instance, the crystal surface mirror typically requires substantial surface preparation and maintenance processes such as annealing, ultrahigh vacuum, and possibly low surface temperature of 100 K. Although these mirrors can work for atoms and molecules, their lifetime is less than ten hours even in ultrahigh vacuum of  $10^{-10}$  mbar.<sup>38,39</sup> To overcome this limitation efforts have been made to stabilize crystal surfaces by coating them with a graphene monolayer. The maximum reflectivity of monolayer



graphene-coated Ru [MLG/Ru(0001)] at 100 K is approximately 20% for He atoms, which can be recovered by annealing to 450 K even after being exposed to air.<sup>40</sup> Electromagnetic-field mirrors can reflect thermal energy atoms under grazing incidence conditions with reflectivity close to 100%.<sup>41,42</sup> But they lack the robustness and compactness of solid mirrors. As for quantum-reflection mirrors their reflectivity approaches unity for extreme grazing incidence, but it readily decreases with increasing incidence angle. MEDR mirrors require nano-fabrication (nanoscale ridged surface) or have low reflectivity for a mirror (400  $\mu\text{m}$ -period grating). Bulky and low-reflectivity mirrors get less suitable as the number of mirrors in an instrument increases. Delicate prerequisites in manufacturing, preparing, and maintaining processes make a mirror expensive. Therefore, these mirrors are not well established in matter-wave optical instruments.

A robust, compact, and, ideally, inexpensive mirror with near 100% reflectivity for atoms and molecules would expedite the development of neutral-particle matter-wave instruments, such as microscopes and interferometers, paralleling applications of conventional mirrors in the wide variety of optical systems used in science and technology.

Here, we show that a commercial blazed grating with sub-micrometer period can function as a mirror for He atoms with a reflection probability of up to about 50%. While the reflectivity of this grating decreases slowly as the incidence angle increases, it still remains above 10% even when the incidence angle is 4 mrad. To determine the underlying reflection mechanism of this mirror, we measure the specular reflection efficiencies of three blazed gratings with different periods for He atomic beams under grazing incidence. The trends of the observed reflection probabilities for the gratings with different periods are qualitatively explained by the MEDR model.<sup>34,37</sup> Comparison of the experimental results obtained with plane-ruled and holographic gratings of identical period but different microscopic and macroscopic shapes allows us to study how these properties affect their performance as mirrors. In addition, by using the mirrors to reflect fragile helium clusters,  $\text{He}_2$  and  $\text{He}_3$ , with high reflectivity, we demonstrate that the new mirror can work for more complex and delicate particles as well.

## 2 Method

Fig. 1(a) and (b) show schematics of the blazed gratings and the experimental setup, respectively (see ESI†<sup>43</sup> for details). In brief, the molecular beam of mean de Broglie wavelength  $\lambda_{\text{dB}}$  (327, 164, and 109 pm for He,  $\text{He}_2$ , and  $\text{He}_3$ ) is produced by supersonic expansion of pure He gas from a source reservoir with stagnation pressure  $P_0$  and temperature  $T_0$ . At  $T_0 = 9.0$  K, we set  $P_0$  to 0.5 and 2 bar for the atom and cluster experiments, respectively. The beam is collimated by two 20  $\mu\text{m}$  wide slits (Slit 1 and Slit 2) before it scatters off the commercial optical grating. We investigate four blazed gratings: three plane-ruled gratings and one holographic grating. Grating periods ( $d$ ) range from 417 nm to 20  $\mu\text{m}$  and nominal blaze angles ( $\gamma$ ) range from  $0.8^\circ$  to  $16.8^\circ$  [see Fig. 1(a)]. An angular spectrum of the incident or reflected beam is measured by precisely rotating the homemade mass spectrometer equipped with an entrance slit (Slit 3). As shown in the inset of Fig. 1(b), in the plane of incidence formed by the incident wavevector and grating normal, we define the incidence angle  $\theta_{\text{in}}$  and detection angle  $\theta_{\text{det}}$  with respect to



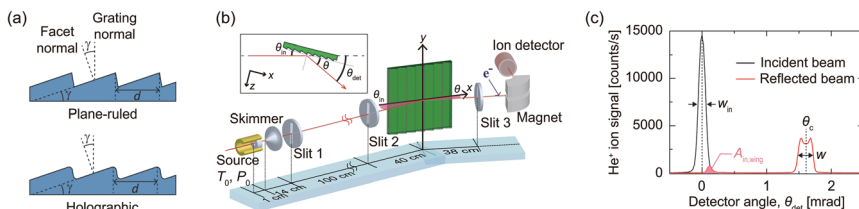


**Fig. 1** (a) Schematics of plane-ruled and holographic gratings. (b) Schematic of the experimental setup; the inset shows the diffraction configuration in the plane of incidence along with the incidence angle ( $\theta_{\text{in}}$ ), detection angle ( $\theta$ ), and detector angle ( $\theta_{\text{det}}$ ). (c) Spectra of the incident (black) and reflected (red) beams. The angular distribution is indicated by a plot of the  $\text{He}^+$  signal as a function of the detector angle  $\theta_{\text{det}}$ , i.e., the angle between the incident beam and the detector position.

the grating plane and the incident beam axis, respectively. Examples of measured incident and reflected spectra are shown in Fig. 1(c). From these angular profiles we determine the widths ( $w_{\text{in}}$  and  $w$ ) and areas ( $A_{\text{in}}$  and  $A$ ) of the incident and reflected beam together with  $\theta_{\text{in}}$ . For specular reflection  $\theta_{\text{in}} = \theta_{\text{c}}/2$ , where  $\theta_{\text{c}}$  is the central angle of the reflected peak indicated in Fig. 1(c). See ESI†<sup>43</sup> for details of data analysis.

### 3 Results and discussion

In our first experiment, we study the underlying reflection mechanism of the gratings by comparing the measured reflectivity for the three plane-ruled gratings of period  $d = 20 \text{ }\mu\text{m}$ ,  $3.3 \text{ }\mu\text{m}$ , and  $417 \text{ nm}$  as a function of  $\theta_{\text{in}}$  with the behavior predicted by the MEDR mechanism as shown in Fig. 2. For each grating, the reflectivity increases with decreasing  $\theta_{\text{in}}$  (except for the smallest  $\theta_{\text{in}}$  values). At any  $\theta_{\text{in}}$  the reflectivity increases as the period decreases (except for the smallest  $\theta_{\text{in}}$  values). We apply the MEDR model by approximating the blazed grating by an array of parallel half-planes, as depicted in Fig. 2(a), and introduce the universal

parameter  $u = \sqrt{\frac{2d}{\lambda}} \sin \frac{\theta_{\text{in}}}{2}$  of the MEDR mechanism. In this model, the efficiency of specular reflection from the structure approaches unity as  $u$  approaches zero, as shown in Fig. 2(b). Therefore, a decrease in  $\theta_{\text{in}}$  or  $d$  reduces  $u$ , leading to stronger reflection. This trend qualitatively agrees with the experimental results for the three gratings. Note that, for the given geometry of the gratings, the largest  $\theta_{\text{in}}$  is much smaller than the blaze angle  $\gamma$ . Thus, specular reflection cannot result from reflection at the grating facets, but can only result from scattering at the edges.

To study how the microscopic and macroscopic properties of a grating affect its reflectivity and the width of the reflected beam, we compare two series of experimental results for plane-ruled and holographic blazed gratings with  $d = 417 \text{ nm}$  (Fig. 3). We choose the gratings of the shortest period since their largest reflectivity is desirable for future usage. According to the manufacturer, holographic gratings, inherently, show fewer periodic errors, spacing errors, and surface irregularities than plane-ruled gratings. AFM images of the two gratings (see Fig. S1 in ESI†<sup>43</sup>) confirm that the edges of the holographic grating are



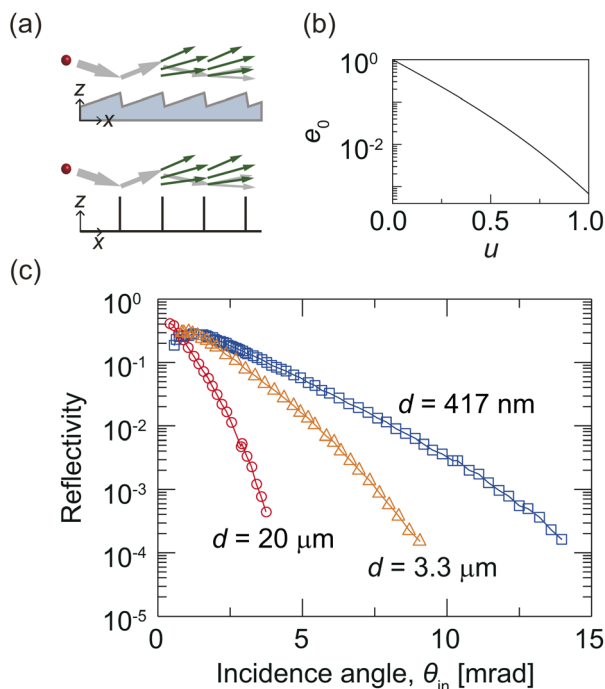


Fig. 2 (a) Sketch of multiple diffraction of atoms at the edges of a grating. We approximate the grating edges by half-planes (indicated by black bars). (b) Specular reflection efficiency  $e_0$  predicted by the multiple edge-diffraction reflection (MEDR) model. The efficiency is plotted as a function of the universal parameter  $u$ . (c) The experimental reflectivities of the gratings as a function of incidence angle  $\theta_{in}$ .

smoother than those of the plane-ruled grating. The standard deviations of edge heights for the holographic and plane-ruled gratings are observed to be 10 and 19 nm, respectively. Furthermore, their macroscale flatness (over the entire grating area) is different. The plane-ruled grating appears to be effectively flat, with an average radius of curvature greater than 2000 m. In contrast, the holographic grating exhibits a convex overall shape corresponding to a radius of curvature of  $\sim 500$  m. See ESI†<sup>43</sup> for details of the grating characterization results.

The holographic grating exhibits higher reflectivity for He atoms than the plane-ruled grating over the entire range of  $\theta_{in}$  from 0.5 to 15 mrad, as demonstrated in Fig. 3(a). We attribute this to the fact that the edges of the holographic grating are more homogeneous than those of its ruled counterpart. In particular, the reflectivity decrease observed for the smallest incidence angles ( $\theta_{in} < 1$  mrad) might result from microscopic imperfections in the plane-ruled grating that are absent for the holographic grating, which has a more regular shape. The maximum reflection probability reaches 47% at  $\theta_{in} = 0.82$  mrad, which is 2.5 times greater than the MLG/Ru(0001) mirror based on the classical reflection mechanism.<sup>40</sup>

Note that under maximum reflection conditions, the reflected beam differs in shape compared to the incident beam, with an increased peak width (namely,  $w > w_{in}$ ), as shown in Fig. 1(c). The wider peak width implies that the grating surface is



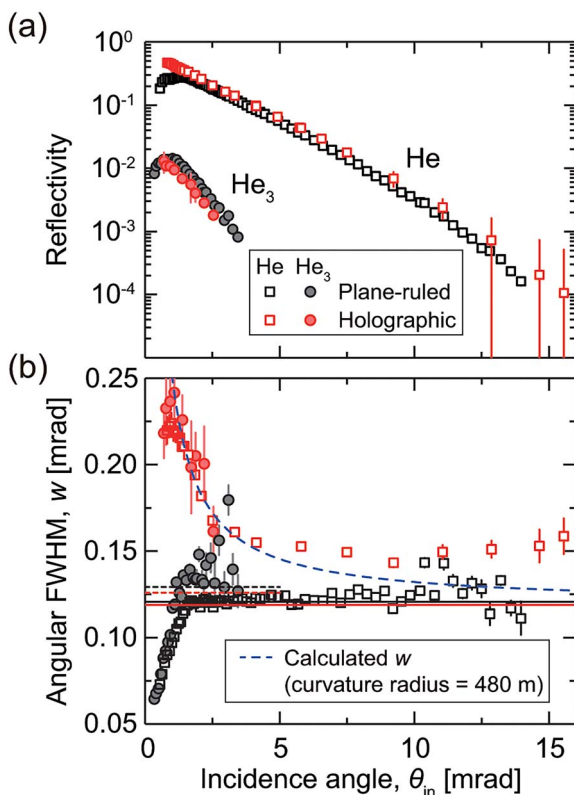


Fig. 3 Comparisons of the experimental results achieved with the plane-ruled and holographic gratings with  $d = 417$  nm. The results for the plane-ruled grating are colored black, and those for the holographic grating are colored red. (a) Reflectivities for He atoms (open squares) and clusters (filled circles) from the two gratings. (b) Angular widths  $w$  (FWHM) for the atoms and clusters measured with increasing  $\theta_{in}$ . The horizontal solid (dotted) lines represent the widths of the incident atom (cluster) beam,  $w_{in}$ , for each series of experiments. Vertical bars represent the uncertainties resulting from Gaussian fitting processes. The blue dashed curve indicates the calculated  $w$  values for a cylindrical convex mirror with a curvature radius of 480 m.

not macroscopically flat. The macroscopic curvature of the holographic grating accounts for the increased peak width. Fig. 3(b) shows the variation in  $w$  with  $\theta_{in}$  for the two gratings. The change in  $w$  for the holographic grating confirms the convex shape of the nominally flat grating in agreement with the AFM results. The measured width agrees reasonably well with the calculated width at  $\theta_{in} < 5$  mrad.<sup>44</sup> However, since the radius of curvature of the grating is ill-defined (see Fig. S2(f) in ESI†<sup>43</sup>) and the alignment among the three slits and the grating plane [see Fig. 1(a)] is not perfect, we do not expect agreement over the entire  $\theta_{in}$  range. If the grating were concave,  $w$  would have shown a minimum at a certain incidence angle.<sup>28</sup>

In contrast, the width of the beam reflected from the plane-ruled grating is close to  $w_{in}$  [black horizontal line in Fig. 3(b)] at  $\theta_{in} > 1.6$  mrad (open squares), which is expected for reflection from a flat surface. For  $\theta_{in} < 1.6$  mrad, the





projected width of the grating is smaller than the width of the collimated incident beam, so only a part of the incident beam hits the grating. This fraction of the beam increases with  $\theta_{\text{in}}$ . This partial reflection explains the decrease in  $w$  at  $\theta_{\text{in}} < 1.6$  mrad.

These observations confirm that the gratings function as efficient mirrors for He atoms under grazing incidence conditions. In particular, the 417 nm-period gratings can work as mirrors whose performance depends on their macroscopic and microscopic properties, such as macroscopic curvature and surface irregularities.

Knowing that optical gratings can work as a good mirror for He atoms, we investigate their performance for small helium clusters,  $\text{He}_2$  and  $\text{He}_3$ . As a result of the extremely small binding energies of  $\text{He}_2$  and  $\text{He}_3$  (0.15  $\mu\text{eV}$  (ref. 45) and 11.4  $\mu\text{eV}$  (ref. 46), respectively), they represent ideal model systems for studying non-destructive scattering of weakly-bound or metastable particles. For instance, classical reflection would lead to break-up of fragile He clusters, de-excite metastable atoms, or annihilate antihydrogen atoms. We utilized the plane-ruled and holographic blazed gratings with  $d = 417$  nm to reflect a mixture of He clusters, mainly  $\text{He}_3$  with a small amount of  $\text{He}_2$ . In Fig. 3(a) and (b), the black and red filled circles represent the reflectivity and peak widths observed for the clusters reflected from the plane-ruled and holographic gratings, respectively. The mirror reflectivity for clusters is found to be lower than that for He atoms. We attribute this to the fact that the de Broglie wavelength of  $\text{He}_3$  in the helium beam is three times shorter than that of He, thereby increasing  $u$  which is inversely proportional to  $\sqrt{\lambda}$ . Although the reflectivity for  $\text{He}_3$  is not as high as that for He atoms, the substantial reflectivity is expected to facilitate further studies with these fragile particles.

Regarding the peak widths, the variations in  $w$  for the helium clusters closely follow those observed for He atoms. This confirms that the width variation is independent of the particle type, and depends solely on the grating's macroscopic shape.

The macroscopic curvature of a grating-type mirror for matter waves is significant in two ways. First, the low peak height of a broadened beam results in a reduction in the signal-to-noise (S/N) ratio. Therefore, a simple reflection experiment with a low reflectivity for the particle would suffer from a small S/N value when the mirror is curved. A planar grating over a range of a few centimeters is thus favorable for such an experiment. Second, we can exploit the grating curvature to focus an incident beam. A concave grating with a properly tailored radius of curvature resulting in a focal length of tens of centimeters works as a concave mirror in matter-wave optics. The high reflectivity of a grating-type mirror facilitates an advanced Kirkpatrick–Baez (AKB) geometry for matter waves that allows tight beam focusing under grazing incidence conditions and requires four reflections.<sup>47,48</sup> For example, if each mirror's reflectivity is 80, 50, or 20%, the intensity of the beam focused by the AKB system is 41, 6.3, or 0.16% of the incident beam intensity. The performance of an AKB system consisting of four grating MEDR mirrors of 50% reflectivity would, hence, be forty times better than one with four MLG/Ru mirrors. Therefore, an AKB microscope using the reflection of neutral helium atoms from concave gratings could complement the other types of scanning helium microscopes that have been demonstrated thus far based on a Fresnel zone plate<sup>10–13,49</sup> and a pinhole.<sup>5,8,50,51</sup>





## 4 Conclusions

In conclusion, we demonstrated that commercially available plane-ruled or holographic blazed gratings can serve as mirrors for matter waves under grazing incidence conditions. The maximum reflection probability is as high as approximately 50% for a 417 nm-period holographic grating. Moreover, we applied this grating to reflect fragile He<sub>2</sub> and He<sub>3</sub> molecules, which readily dissociate upon colliding with a flat surface. Our results imply that reflection from grating mirrors *via* the MEDR mechanism offers a general approach that could be used with other fragile or metastable particles, such as antihydrogen atoms, for example. However, inherent imperfections of the grating edges on the microscale and the deviation from flatness of our gratings on the macroscale reduce the performance of the gratings as a mirror and cause the reflection probability to deviate from the MEDR model predictions. In the future, we can improve the quality of the gratings as mirrors by reducing the period, minimizing periodic errors and edge roughness, and maintaining an appropriate macroscopic surface flatness. Furthermore, a fine grating with a well-defined macroscopic curvature could function as an excellent focusing element. These findings can, therefore, pave the way for developing improved microscopes and interferometers that use atomic or molecular matter waves.

## Author contributions

B. S. Z. and W. S. conceived and supervised the experiment. B. S. Z., D. W. K., S. P., S. L., and J. W. K. performed the measurements. L. Y. K., D. W. K., and B. S. Z. analyzed the data. B. S. Z. and W. S. wrote the manuscript with input from L. Y. K. and D. W. K.

## Conflicts of interest

There are no conflicts to declare.

## Acknowledgements

This work was supported by NRF (National Research Foundation of Korea) grants funded by the Korean government (NRF-2019R1A2C1086215, NRF-2020R1A2C3003701, NRF-2022R1A4A1033247, and NRF-2017H1A2A1042369).

## Notes and references

- 1 C. Davisson and L. H. Germer, *Nature*, 1927, **119**, 558–560.
- 2 I. Estermann and O. Stern, *Z. Phys.*, 1930, **61**, 95–125.
- 3 M. Knoll and E. Ruska, *Z. Phys.*, 1932, **78**, 318–339.
- 4 A. S. Palau, S. D. Eder, G. Bracco and B. Holst, *Ultramicroscopy*, 2023, **251**, 113753.
- 5 P. Witham and E. Sánchez, *Rev. Sci. Instrum.*, 2011, **82**, 103705.
- 6 P. J. Witham and E. J. Sanchez, *J. Microsc.*, 2012, **248**, 223–227.
- 7 P. Witham and E. Sanchez, *Cryst. Res. Technol.*, 2014, **49**, 690–698.
- 8 M. Barr, A. Fahy, J. Martens, A. P. Jardine, D. J. Ward, J. Ellis, W. Allison and P. C. Dastoor, *Nat. Commun.*, 2016, **7**, 10189.



- 9 A. Fahy, S. Eder, M. Barr, J. Martens, T. Myles and P. Dastoor, *Ultramicroscopy*, 2018, **192**, 7–13.
- 10 O. Carnal, M. Sigel, T. Sleator, H. Takuma and J. Mlynek, *Phys. Rev. Lett.*, 1991, **67**, 3231–3234.
- 11 R. B. Doak, R. E. Grisenti, S. Rehbein, G. Schmahl, J. P. Toennies and C. Wöll, *Phys. Rev. Lett.*, 1999, **83**, 4229–4232.
- 12 T. Reisinger, S. Eder, M. M. Greve, H. I. Smith and B. Holst, *Microelectron. Eng.*, 2010, **87**, 1011–1014.
- 13 S. D. Eder, T. Reisinger, M. M. Greve, G. Bracco and B. Holst, *New J. Phys.*, 2012, **14**, 073014.
- 14 A. D. Cronin, J. Schmiedmayer and D. E. Pritchard, *Rev. Mod. Phys.*, 2009, **81**, 1051–1129.
- 15 *Helium Atom Scattering from Surfaces*, ed. E. Hulpke, Springer, Berlin, 1992.
- 16 D. Fariás and K. H. Rieder, *Rep. Prog. Phys.*, 1998, **61**, 1575.
- 17 T. M. Roach, H. Abele, M. G. Boshier, H. L. Grossman, K. P. Zetie and E. A. Hinds, *Phys. Rev. Lett.*, 1995, **75**, 629–632.
- 18 H. Merimeche, *J. Phys. B: At., Mol. Opt. Phys.*, 2006, **39**, 3723–3731.
- 19 M. Metsälä, J. J. Gilijamse, S. Hoekstra, S. Y. T. van de Meerakker and G. Meijer, *New J. Phys.*, 2008, **10**, 053018.
- 20 S. A. Schulz, H. L. Bethlem, J. van Veldhoven, J. Küpper, H. Conrad and G. Meijer, *Phys. Rev. Lett.*, 2004, **93**, 020406.
- 21 M. A. Kasevich, D. S. Weiss and S. Chu, *Opt. Lett.*, 1990, **15**, 607–609.
- 22 V. U. Nayak, D. O. Edwards and N. Masuhara, *Phys. Rev. Lett.*, 1983, **50**, 990–992.
- 23 I. A. Yu, J. M. Doyle, J. C. Sandberg, C. L. Cesar, D. Kleppner and T. J. Greytak, *Phys. Rev. Lett.*, 1993, **71**, 1589–1592.
- 24 J. J. Berkhout, O. J. Luiten, I. D. Setija, T. W. Hijmans, T. Mizusaki and J. T. M. Walraven, *Phys. Rev. Lett.*, 1989, **63**, 1689–1692.
- 25 F. Shimizu, *Phys. Rev. Lett.*, 2001, **86**, 987–990.
- 26 V. Druzhinina and M. DeKieviet, *Phys. Rev. Lett.*, 2003, **91**, 193202.
- 27 T. A. Pasquini, Y. Shin, C. Sanner, M. Saba, A. Schirotzek, D. E. Pritchard and W. Ketterle, *Phys. Rev. Lett.*, 2004, **93**, 223201.
- 28 H. C. Schewe, B. S. Zhao, G. Meijer and W. Schöllkopf, *New J. Phys.*, 2009, **11**, 113030.
- 29 B. S. Zhao, H. C. Schewe, G. Meijer and W. Schöllkopf, *Phys. Rev. Lett.*, 2010, **105**, 133203.
- 30 F. Shimizu and J. Fujita, *J. Phys. Soc. Jpn.*, 2002, **71**, 5–8.
- 31 T. Pasquini, M. Saba, G. Jo, Y. Shin, W. Ketterle, D. Pritchard, T. Savas and N. Mulders, *Phys. Rev. Lett.*, 2006, **97**, 093201.
- 32 H. Friedrich, G. Jacoby and C. G. Meister, *Phys. Rev. A: At., Mol., Opt. Phys.*, 2002, **65**, 032902.
- 33 J. Petersen, E. Pollak and S. Miret-Artés, *Phys. Rev. A*, 2018, **97**, 042102.
- 34 E. Bogomolny and C. Schmit, *Nonlinearity*, 2003, **16**, 2035–2059.
- 35 H. Oberst, D. Kouznetsov, K. Shimizu, J. Fujita and F. Shimizu, *Phys. Rev. Lett.*, 2005, **94**, 013203.
- 36 D. Kouznetsov and H. Oberst, *Phys. Rev. A: At., Mol., Opt. Phys.*, 2005, **72**, 013617.
- 37 J. H. Lee, L. Y. Kim, Y.-T. Kim, C. Y. Lee, W. Schöllkopf and B. S. Zhao, *Phys. Rev. Lett.*, 2019, **122**, 040401.



- 38 D. Barredo, F. Calleja, A. Weeks, P. Nieto, J. Hinarejos, G. Laurent, A. V. de Parga, D. MacLaren, D. Farías, W. Allison and R. Miranda, *Surf. Sci.*, 2007, **601**, 24–29.
- 39 G. Anemone, A. A. Taleb, S. D. Eder, B. Holst and D. Farías, *Phys. Rev. B*, 2017, **95**, 205428.
- 40 A. Politano, B. Borca, M. Minniti, J. J. Hinarejos, A. L. Vázquez de Parga, D. Farías and R. Miranda, *Phys. Rev. B: Condens. Matter Mater. Phys.*, 2011, **84**, 035450.
- 41 V. I. Balykin, V. S. Letokhov, Y. B. Ovchinnikov and A. I. Sidorov, *J. Exp. Theor. Phys.*, 1987, **45**, 353–356.
- 42 V. I. Balykin, V. S. Letokhov, Y. B. Ovchinnikov and A. I. Sidorov, *Phys. Rev. Lett.*, 1988, **60**, 2137–2140.
- 43 See ESI† for the details of the gratings, the experimental setup, and the data analysis.
- 44 L. Y. Kim, D. W. Kang, J. C. Lee, E. Chae, W. Schöllkopf and B. S. Zhao, *arXiv*, 2023, preprint, arXiv:2311.12416, DOI: [10.48550/arXiv.2311.12416](https://doi.org/10.48550/arXiv.2311.12416).
- 45 S. Zeller, M. Kunitski, J. Voigtsberger, A. Kalinin, A. Schottelius, C. Schober, M. Waitz, H. Sann, A. Hartung, T. Bauer, M. Pitzer, F. Trinter, C. Goihl, C. Janke, M. Richter, G. Kastirke, M. Weller, A. Czasch, M. Kitzler, M. Braune, R. E. Grisenti, W. Schöllkopf, L. P. H. Schmidt, M. S. Schöffler, J. B. Williams, T. Jahnke and R. Dörner, *Proc. Natl. Acad. Sci. U. S. A.*, 2016, **113**, 14651–14655.
- 46 E. Hiyama and M. Kamimura, *Phys. Rev. A: At., Mol., Opt. Phys.*, 2012, **85**, 062505.
- 47 R. Kodama, N. Ikeda, Y. Kato, Y. Katori, T. Iwai and K. Takeshi, *Opt. Lett.*, 1996, **21**, 1321–1323.
- 48 R. Sauneuf, J.-M. Dalmaso, T. Jalinaud, J.-P. Le Breton, D. Schirmann, J.-P. Marioge, F. Bridou, G. Tissot and J.-Y. Clotaire, *Rev. Sci. Instrum.*, 1997, **68**, 3412–3420.
- 49 R. Flatabø, M. M. Greve, S. D. Eder, M. Kalläne, A. S. Palau, K. K. Berggren and B. Holst, *J. Vac. Sci. Technol., B*, 2017, **35**, 06G502.
- 50 M. Bergin, S. M. Lambrick, H. Sleath, D. J. Ward, J. Ellis and A. P. Jardine, *Sci. Rep.*, 2020, **10**, 2053.
- 51 G. Bhardwaj, K. R. Sahoo, R. Sharma, P. Nath and P. R. Shirhatti, *Phys. Rev. A*, 2022, **105**, 022828.

